

International Journal of Scientific Research and Reviews

A Study on Structural, Optical and Electrical Properties of V₂O₅ Nanorods by Simple Wet Chemical Method

R. Thangarasu^a and O .N. Balasundaram^{a*}

^(a) Department of Physics, PSG College of Arts & Science, Coimbatore- 641 014, Tamilnadu, India
Tel: 0422 430 3320; Fax: +91-04224303300;E-Mail: nbalasundarm@gmail.com

ABSTRACT

We report the synthesis of V₂O₅nanoparticlesby utilizing simple wet chemical method. The achieve of preparation and characterization by XRD, HR-TEM, UV, PL, FTIR, AC, DC conductivity studies. The X-ray diffraction analysis revealed that the prepared sample annealed at 600 °C for 1 hrs. This exhibited that orthorhombic phase of V₂O₅nanoparticles. The powders are characterized for optical properties by studying the optical absorption spectra in the wavelength range 200-1000 nm at room temperature using UV-vis spectrometer. The V₂O₅nanoparticles produced by this technique are single crystalline and could emit intense visible light at room temperature, possibly due to some defects such as oxygen vacancies which got involved during growth. FTIR spectrum confirmed that the presence of V₂O₅ function group and the formation of V-O bond system. The HR-TEM images dense, smooth and random distribution of V₂O₅nanoparticles and high surface roughness, RMS value for found out. Further, the AC conductivity follows the Jonscher power law and keeps a constant value at low frequencies before a rapid increase in high frequencies owing to hopping mechanism in the conduction process. The DC electrical conductivity was studies as a function of temperature which indicated the semiconductor nature.

KEY WORDS:V₂O₅, XRD, Optical, morphological, AC, DC conductivity

***Corresponding author**

Dr. O.N. Balasundaram,

Associate Professor,Department of Physics,

PSG College of Arts and Science,

Coimbatore- 641014,

Tamilnadu, India

E-Mail: nbalasundarm@gmail.com

1. INTRODUCTION

Vanadium pentoxide (V_2O_5) due to its excellent and unique physical and chemical properties as a semiconductor material. V_2O_5 is the saturated (highest oxidation state) oxide, and therefore the most stable one, in the V–O system¹. Vanadium occurs as a single valence in oxidation states from V^{2+} to V^{5+} , in the form of different phases (VO , VO_2 , V_2O_3 , V_4O_9 and V_2O_5) and a number of mixed-valence oxides (V_6O_{13} , $V_{10}O_{24}$). Though the presence of various phases, single or multiple valence states and different layered structures (vanadium oxides) can be described from the application point of view, a single phase V_2O_5 is more suitable and its practical importance of great interest in different fields of science and technology. Among them V_2O_5 is mostly studied and it is considered to be a prominent n-type semiconductor with wide direct band gap (2.42 eV)². And attracts continuing attention owing to its great potential in a wide variety of scientific and technological applications in recent years. They find extensive applications in areas such as high energy lithium batteries³, catalysis⁴, solar cells⁵ and field effect transistors (FETs)⁶. Now days, one-dimensional (1D) - V_2O_5 nano structures such as nano wires, nano belts nano spindle and nano rods gain notice considerably due to their unique properties towards electronic and optoelectronic application. Among the 1D- V_2O_5 is perhaps the most studied, owing to its features like in expensive preparation, high stability and the significantly large energy density. During the past decades, a variety of methods such as reverse-micelles synthesis⁷, sol-gel method⁸, hydrothermal⁹, chemical vapor deposition¹⁰, thermal-decomposition¹¹, pulsed laser deposition¹² and electro-spinning¹³ are commonly used to prepare 1D- V_2O_5 nano structures. Compared with these methods, sol-gel synthetic route holds the advantage of easier control of the morphological parameters of nano materials and does not require any sophisticated equipment's. Avansi et al. recently reported an environmentally one step hydrothermal route for synthesis of V_2O_5 nanostructure¹⁴. Muster et al. studied the electrical transport mechanism route for synthesis of V_2O_5 nano fibers in detail¹⁵. Ferrer-anglada et al. analysed the current-voltage (I-V) Characteristics and electrical resistance was measured on V_2O_{5-x} polyaniline nanorods¹⁶. This work, we studied the effect of temperature on structural and optical properties of 1D-nanoparticles by the sol-gel method. Synthesis of V_2O_5 nanorods by this method exhibits much better optical, morphological and electrical properties than commercial nanosized V_2O_5 . Further the nano particles were characterized by various techniques and the characterization results are discussed in details.

2. EXPERIMENTAL PROCEDURE

All of the chemicals were used in the experiment were of analytical reagent (AR) grade and used without any further purification. The ammonium meta vanadate (NH_4VO_3), hydrogen peroxide

(H₂O₂), nitric acid (HNO₃), Polyvinylpyrrolidone (PVP), purchased from Merck company, was used as the precursor materials for synthesis of V₂O₅ nanoparticles by wet chemical method. The flow chart of the preparation of V₂O₅ nanoparticles is shown in Fig. 1. In a typical synthesis procedure, an appropriate amount of ammonium meta vanadate (NH₄VO₃) was dissolved in deionised water and stirred for 10–30 min at room temperature. In the aqueous solution contains a milky white color was precipitated then a given amount of 10ml 35% H₂O₂ was added, quickly the milky white color changed to light pale yellow shade. Upon an introduction of aliquot concentrated Hcl acid was into the system, the color of the reaction mixture changed from pale yellow to dark orange color¹⁷. Finally, a desired amount of Polyvinylpyrrolidone (PVP) was added into concoction solution under vigorous stirring for 24h. In the resulting pale yellow gel form was filtered, washed with deionised water and absolute ethanol, and acetone dried at 90°C for 6h to get as-prepared sample. Then dried product was transferred to a silicon crucible for purpose of sintering and placed in muffle furnace used at temperatures, say 600°C for 1 h till yellow colored V₂O₅ nano-particles were obtained.

3. CHARACTERIZATION TECHNIQUES

The crystal structural characterization of the V₂O₅ nanoparticles was performed by X-ray diffraction using a Bruker AXS D8 advance diffractometer with Cu-K α radiation source $\lambda=1.5406$ Å. The absorption spectrum studies are also done using UV–vis–NIR spectro photo meter between 200 and 1000 nm (Jasco V-570). The Spectro flurometer spectrum is examined by the instrument model of Jobin Yvon Fluoromax of 185–900nm. The Fourier transform infrared (FT-IR) (Perkin Elmer 100) is used to record the spectra range from 400 to 4000 cm⁻¹ with are solution of 4cm⁻¹. The structure and morphology of nanorods were examined using High-Resolution Transmission Electron Microscopy (JEOL JEM-2100, HRTEM, and Japan). Dielectric measurements were carried out in the frequency range 42 Hz to 5 MHz using LCR HI-Tester (HIOKI 3532-50). DC conductivity studies were performed in the temperature range 30-130°C and measurements were carried out using a Keithley 6517 B electrometer.

4. RESULTS AND DISCUSSION

4.1 XRD-Analysis

Fig.1 (a) demonstrates the XRD pattern of the V₂O₅ nanoparticles prepared in surfactants solutions. Xrd pattern of PVP capped V₂O₅ nanorods. No excess peaks, which indicate that all the precursors have been completely decomposed and no other complex products were formed. All the diffraction peaks are indexed with the pure orthorhombic phase of V₂O₅ nanoparticles with the lattice parameters a=11.207 Å, b=3.537 Å and c=4.397 Å (jcpds Card No: 41-1426 space group Pmmn) without any impurity peaks. Furthermore, the crystalline size can be estimated to be 20-55nm, for pure V₂O₅ by using the debye-scherrer formula. The average grain size of calculation at 600°C were

calculated to be 21.68 nm, from the (200), (001), (101),(110),(301),(011),and (310) peaks using the Debye scherrer equation

$$D = \frac{k\lambda}{\beta \cos \theta} \text{-----(1)}$$

$$d = \frac{n\lambda}{2 \sin \theta} \text{-----(2)}$$

Where d is the crystallite size, λ is the X-ray wavelength (1.54 Å), β is full width at half maximum of the high intensity peak and θ is Bragg’s diffraction angle in degrees. It is clear that of V₂O₅ crystalline nature in calcinations temperature at 600°C for crystalline nature to that of 600°C probably due to the formation of structural defects .Notably the sample annealed at 600°C producing a significant improvement in crystallinity, showing more strong and sharper Diffraction peaks as compared to the other sample the number of diffraction line increase in V₂O₅ orientations with temperature increase in the crystallite size¹⁸.

The difference in the estimated crystalline size indicates that the same differences in size and morphology of the V₂O₅ nanoparticles.

The dislocation density which represents the amount of defect in the samples is determined from the formula (3)

$$\zeta = \frac{1}{D^2} \text{-----(3)}$$

$$\varepsilon = \frac{\beta \cos \theta}{4} \text{-----(4)}$$

Where D is the grain size. The dislocation density decreases with increasing annealing temperature which may be due to decrease in concentration of lattice imperfections¹⁹. The influence of particle size on lattice parameter also noticed from XRD pattern. The particle size increases, the value of lattice parameter decreases as shown in Fig.1 (a) and

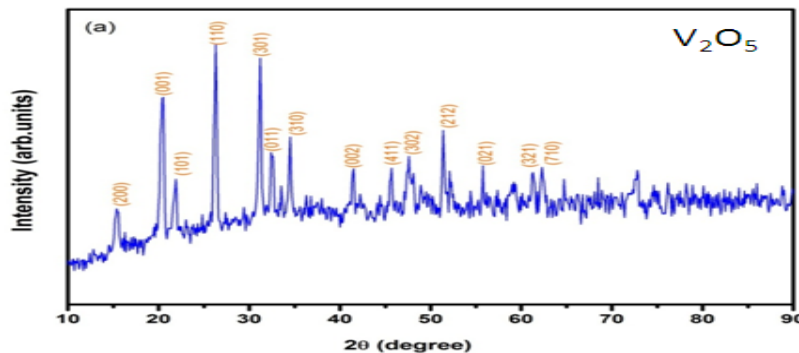


Fig. 1 (a) XRD structure of V₂O₅ sample at 600°C temperature

Table: 1 Structural Parameters of V₂O₅ nanorods

Material	2theta (deg)	(hkl)	FWHM	Lattice parameters	Crystallite size	Dislocation Density (lines/m ²)	Micro strain(ε) (10 ⁻³)	Surface roughness (Ra)	RMS (R _q)
V ₂ O ₅	21.50	(101)	0.5617	a =11.207	14.39 nm	0.0694	0.1379	82.5	108.4
	26.50	(110)	0.3035		26.88nm	0.0372	0.0738		
	31.60	(400)	0.2795	b =3.537	29.53nm	0.0338	0.0670		
	38.50	(401)	0.0764		11.01 nm	0.0908	0.0180		
	40.50	(311)	0.3183	c =4.397	26.60nm	0.0375	0.0746		

Table (1). It is seen from Fig. 1(a), the dislocation density and strain are both decrease when the annealed temperature 600°C. A sharp decrease dislocation density and strain improve the crystallinity of the V₂O₅ nanoparticle is calculated (101) plane.

4.2 UV –Visible Spectroscopy

The UV-visible absorption spectrum of annealed at 600°C of V₂O₅ nanorods is shown in the Fig. 2(a). It can be seen that the excitonic absorption peak of V₂O₅ samples appear around 472.4 nm (E_g =2.64 eV) and it is shows a blue shift in comparison with the bulk V₂O₅ (E_g = 2.34 eV), Which may be ascribed to the quantum confinement effect due to electronic transition from occupied 2p bands of oxygen to unoccupied 3d bands of vanadium²⁰.

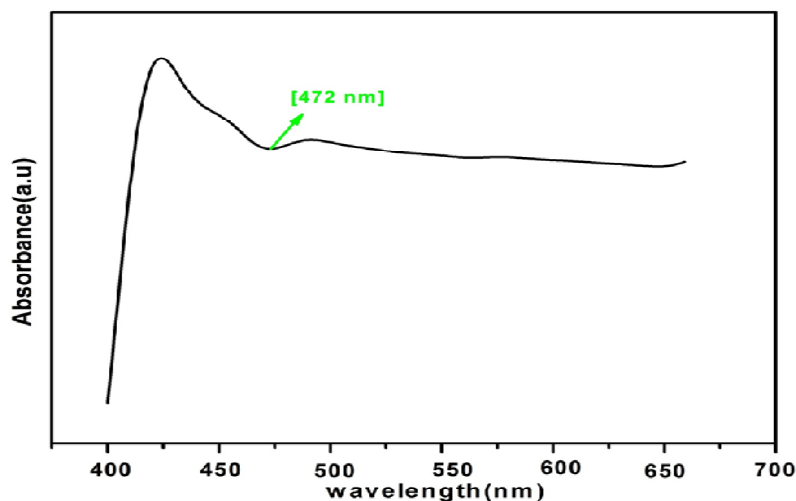


Fig. 2(a) UV-visible absorption spectra of V₂O₅ nanoparticle annealed at 600°C.

It is well-known that the band maxima of the charge transfer transition of O²⁻ → Vⁿ⁺ depends on the number of oxygen atoms surroundings central vanadium ion²¹. Therefore, V⁵⁺ in tetrahedral coordination absorbs in the range 240-350 nm, in square pyramidal coordination at 350-450 nm and in octahedral coordination at 450-600nm. In this spectrum shows a weak band at around 472.4 nm

which can be attributed to lower energy charge transfer to V^{5+} species in octahedral coordination. In the figure it can be observed clearly from the absorbance of the samples decreases slightly with increase in annealing temperature. Furthermore, a red-shift is observed in the characteristics absorption peak of V_2O_5 , the optical bandgap values of the V_2O_5 sample annealed at 600°C temperature to be about 2.64 eV that agrees with the bulk bandgap.

4.3 Photoluminescence Spectroscopy

The optical properties of V_2O_5 nanorods, we carried out PL measurements at room temperature. The PL emission spectra of the V_2O_5 at 600°C annealing temperature are shown in Fig.3 (a). In intact case, it consists of strong blue green emission peak at 435 nm which is originated from there combination of free excitations.

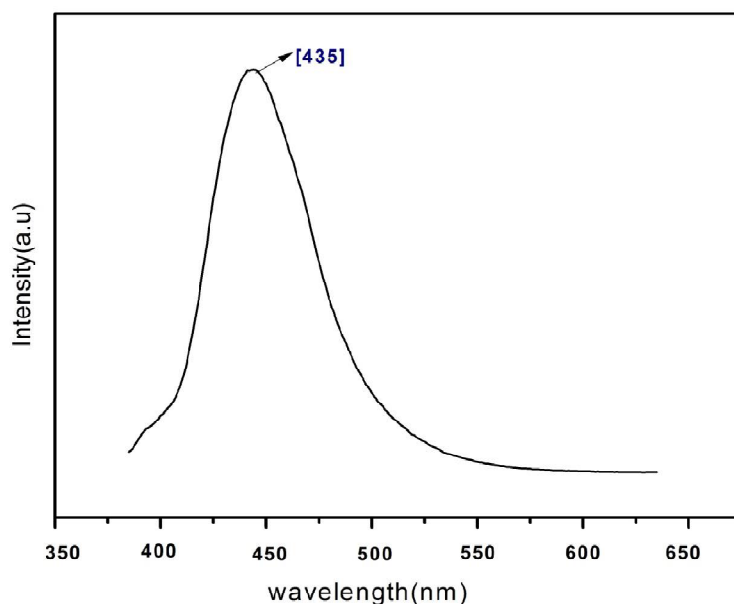


Fig. 3 (a) Photoluminescence spectrum of V_2O_5 annealed at 600°C .

The luminescence at 435 nm may be considered to be related to the signal ionized oxygen vacancy due to the defect in V_2O_5 . The broad emission band revealed in the visible region in our samples is due to the super position of blue-green emission. It was reported that the oxygen vacancies are responsible for the green emission are mainly located at the surface²². As the temperature increase, will be the positions are basically unchanged but the intensity of peak increase which may be attribute to the increase in grain size and crystallinity. The UV and blue-green emission of V_2O_5 nanorods have been broadly studied and the mechanism is also clearly known.

4.4 FTIR-Analysis

The FT-IR spectrum of the V_2O_5 nanoparticles treated at 600°C is shown in Fig. 4(a) the analysis of spectrum contains very broad and strong absorption band centered at 3437 cm^{-1} due to the stretching vibration of the O–H bond. Two sets of vibrational peaks observed at $2934, 2403\text{ cm}^{-1}$ and $1659, 1432\text{ cm}^{-1}$ are related to the characteristic bands of symmetric stretching and scissoring (bending) modes of C–H group, respectively. The absorption peaks at 1741 and 1633 cm^{-1} are due to the stretching vibration modes of C=O group. The V_2O_5 samples exhibits three main vibration modes in the $600\text{--}1020\text{ cm}^{-1}$ region. The terminal oxygen symmetric stretching mode (ν_s) of V=O, the bridge oxygen asymmetric and symmetric stretching modes (ν_{as} and ν_s) of V–O–V are observed at $1017, 824$ and 606 cm^{-1} , respectively²³.

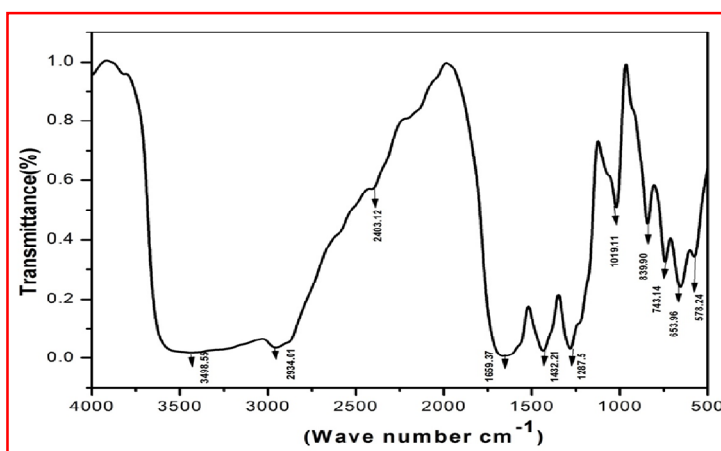


Fig. 4 (a) FT-IR Spectrum of V_2O_5 nanorods for chemical nature of the bonds

In the figure, the V_2O_5 samples annealed at 600°C , the organic bands diminished. It can be deduced that the crystal phase is improved at 600°C , as comparatively a lower annealing temperatures. The organic bands slowly decompose with increasing temperature, so that the crystallization process is essentially complete at 600°C .

4.5 TEM Analysis

Fig. 5(a-d) shows the TEM images V_2O_5 sample annealed at 600°C , which clearly indicated that formation of large size micro-rod particles. The average size and length of individual microrods are about $45\text{--}90\text{ nm}$ and $2\text{--}3\mu\text{m}$, which is in agreement with the SEM result.

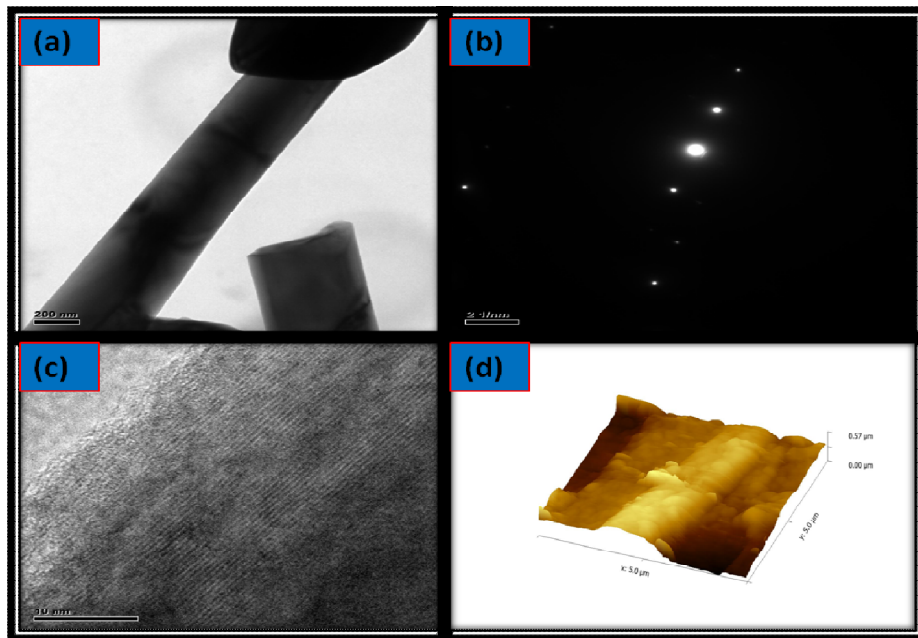


Fig. 5 HRTEM images of (a) V_2O_5 nanorods at annealing temperature at $600^\circ C$ (b) single crystalline V_2O_5 nanorods with SAED pattern (c) Lattice fringes of (001) plane with V_2O_5 (d). AFM images of pure V_2O_5 nanoparticles

We suggest that the nanorods could be grown from the well defined faced end to the hexagonal face end, The selected area electron diffraction (SAED) pattern presented in shown on Fig. 5(b-c) bright spot in the sample, we can see the images of orthorhombic structure of V_2O_5 . In this regard, a significant transition of SAED pattern for the crystalline nature of V_2O_5 sample at $600^\circ C$ is observed²⁴. The fringes images also confirms that the nanorods grow along the (002) direction with a lattice spacing of about 2.14 \AA indicating that the V_2O_5 nanorods is single crystalline in nature. Fig.5(d) surface morphology of the pure V_2O_5 nanoparticles were observed using AFM on linear in the surface roughness is due to the grainsize of the nanopartilces, relatively, large variation in surface roughness and root-mean square (RMS) values are observed for V_2O_5 nanoparticles as evident from table.2

4.6 Electrical Studies

For the electrical measurements of investigated samples were ground into fine powders by agate mortar using a pestle and compressed into pellets of 1 cm diameter and 2 mm thickness by applied pressure of the hydraulic press under a 7 tones/sq.cm for 10 mins. The temperature-dependence of DC conductivity give the information about the long time ion dynamics and it is well described by the Arrhenius law, reflecting the activated nature of ionic hopping processes. At higher frequencies, the conductivity becomes strongly dependent on frequency which varying that approximately as a fractional power of frequency as the Eq(5).

$$\sigma = \sigma_{ac} + \sigma_{dc} = A\omega^s + \sigma_{dc} \quad \text{----- (5)}$$

where, σ_{dc} is the frequency-independent component, A is a temperature dependent constant, s is the frequency exponent and $\sigma_{ac}=A\omega^s$ represents as or dissipative contribution to the total conductivity, which depends on frequency, temperature and composition of the sample

4.6.1 AC conductivity (σ_{ac})

Fig. 6 (a) shows the variation of AC conductivity with temperature and confirms the semiconducting nature of V_2O_5 sample. The conductivity at higher temperatures seems to be frequency independent, while dispersion is observed at lower temperature.

In the dispersion region, the AC conductivity increases with increase of frequency. At lower frequencies, the ions jump from one site to its neighboring vacant site successfully and also contributing to the DC conductivity. At higher frequencies hopping and relaxation of ions give rise to dispersion. After, jumping from one site to the other, the ions can relax in two competing ways as back to its original site or to the neighbouring vacant²⁵. The ions are rearranged in the course of their hopping motion. The relaxation of ions in association with the conduction gives a frequency dispersion region in the conductivity spectra. The increase of (σ_{ac})with temperature is attributed to the increase in the drift mobility and hopping frequency of charge carriers. Generally, the total conductivity is the summation of the band hopping parts of the equation (6),

$$\sigma_{tot} = \sigma_0(T) + \sigma(\omega, T) \text{-----(6)}$$

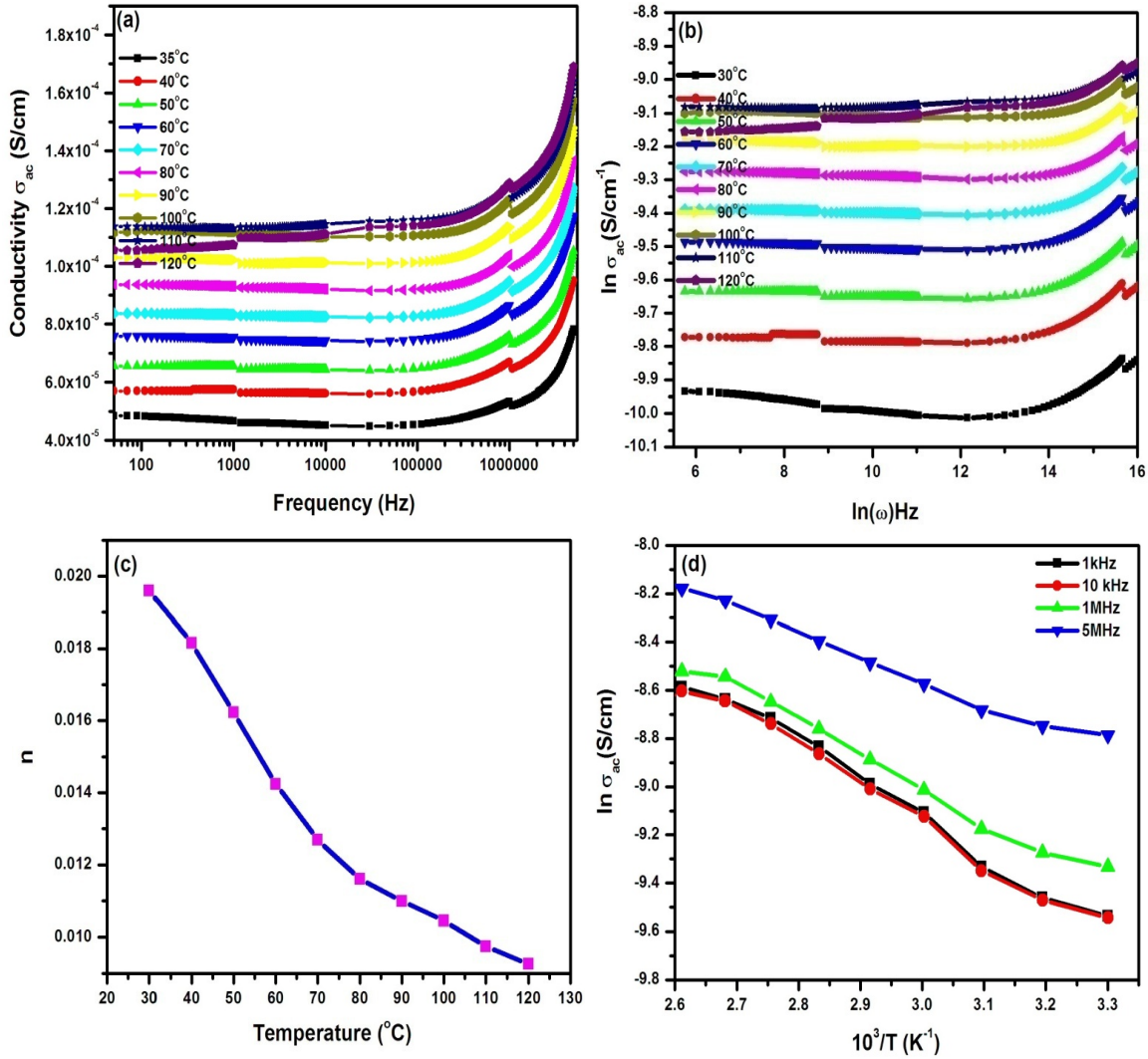


Fig. 6 AC electrical conductivity of (a) V₂O₅, (b) ln (σ_{ac}) vs. ln (ω), (c) plot of exponent n and (d) activation energy with selected applied frequency

The first term in RHS is the DC conductivity due to the band conduction, which is frequency independent. The second term is the pure AC conductivity obeys the empirical formula of the frequency dependence given by the AC power law of the equation (7),

$$\sigma(\omega) = B\omega^n \text{-----(7)}$$

where, B and n are the constants which depend on both temperature and composition, n is the dimensionless quantity, whereas B has the unit of electrical conductivity. The exponent n can be calculated as the function of temperature for each samples by plotting ln (σ) vs. ln (ω) (Fig. 6(b)). Fig. 6(c) shows the variation of n with the different temperature. It is well known that the behaviour

of n with the temperature can be taken as the criterion for the conduction mechanism. The predominant CBH mechanism is confirmed by decreases of n with increase of temperature. The AC conductivity obeys the well-known Arrhenius law (8),

$$\sigma = \sigma_0 \exp\left(-\frac{E_a}{KT}\right) \text{-----(8)}$$

where, E_a is the activation energy required for hopping of charges, T is the absolute temperature and σ_0 is the specific conductivity. In case of low-mobility semiconductors, the activation energy is often connected with the mobility of charge carriers (Fig. 6(d)).

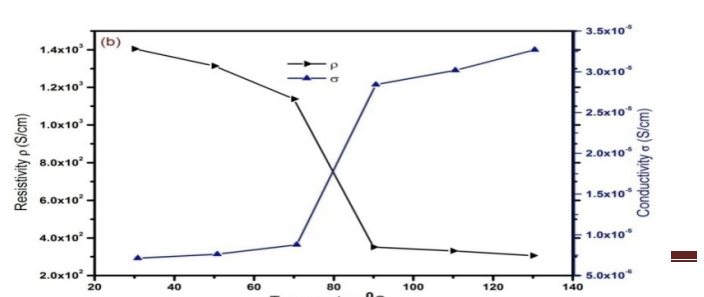
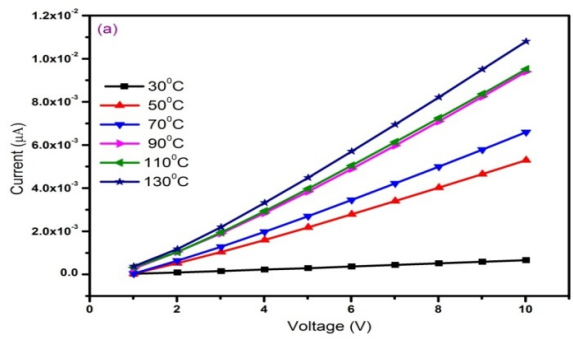
4.6.2 DC Conductivity

I-V characteristics studs low to high level temperatures shown on Fig 7(a) and are found to be linear behaviours from lower temperature. The current in lower voltage range (1-10v) from 30-130°C and in higher voltage range they deviation from the low temperature are indicated ohmic behaviour. It is also evident from Fig.7 (a). The applied voltage are increase with higher temperature .it can be seen that I-V characteristics deviates from non-ohmic behaviour and slowly the resistance goes on decreasing. In order to study the qualitatively this behaviour of material for whole mechanism could be divided into two parts. First one is related to the lower and higher temperature dependence of conductivity and resistance for samples under test²⁶. The second is related with the deviation of ohmic behaviour towards non-ohmic behaviour of I–V characteristics at higher voltages applied across the sample. The conductivity and resistivity of the prepared samples are calculated as from the equation (9)

$$\sigma = \frac{1}{\rho} = \frac{It}{VA} \text{ S/cm} \text{-----(9)}$$

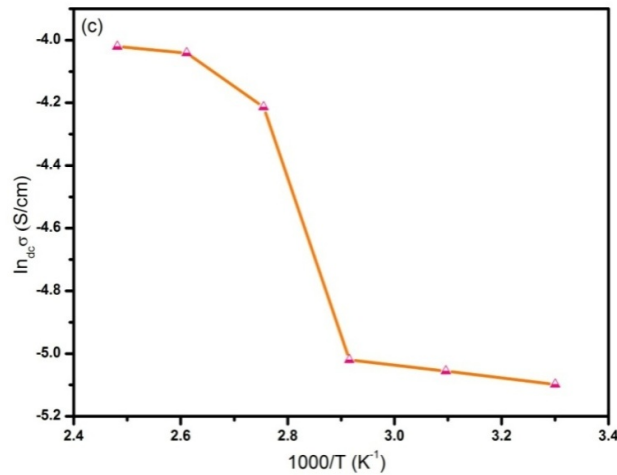
where, I is the current, V is the applied voltage t -is the thickness of the pellet and A -is the area of the pellet, in order to investigate the rectifying behaviour of the V_2O_5 Nanorods. I-V characteristic are obtained by connecting Keithley electrometer to the two probe setup in equation. (10)

Where, ρ is the $\rho = \frac{AR}{l}$ ----- (10) resistivity, R is the resistance, A is the cross sectional area, and l is the inter-probe distance, the



conductivity is computed from have the relation $\sigma = \frac{1}{\rho}$, where σ -is the conductivity

Fig. 7 (a-c) I-V Characteristics (a) V₂O₅ (b) Resistivity decrease and conductivity increase of V₂O₅ nanorods (c) activation energy of ln S dc (S/cm) Vs.103/T K⁻¹



The calculated for conductivity and resistivity are listed in the Table (2). The conductivity is found to be in the range 7.87×10^{-6} to 1.34×10^{-5} S cm⁻¹ for different temperature 30-130°C. It is clear from Fig.7(b) the resistivity decrease with temperature which shows the semiconducting behaviour of the V₂O₅ nano rods. The conductivity increase show to opposite resistivity decreases, show resistivity in order to V₂O₅, was 10^3 Ω/cm at 600°C for V₂O₅ nanorods²⁷.

Table. 2 Electrical parameters of the V₂O₅ nanorods

Material	Resistivity (ρ)Ω cm ⁻¹	Conductivity (σ) S/cm ⁻¹	Activation energy (E_a) eV
V ₂ O ₅	1.34×10^3	7.87×10^{-6}	0.185

The values are in good agreement with the reported values. This may be due to the surfactants of exposed for the maximum solubility in V₂O₅ host lattice, more grain size boundary segregation of impurities that occurring as dispersion of charge carriers, the calculated as

conductivity and resistivity parameter are listed in Table (2). The activation energy are calculated from the Arrhenius relation (11)

$$\sigma = \sigma_0 \exp \left[-E_a / 2K_B T \right] \text{ ----- (11)}$$

Where, σ_0 is the pre exponential factor, E_a is the activation energy, K_B is the Boltzmann constant and T is the absolute temperature. The activation energy of the V_2O_5 for surfactants as V_2O_5 have been used as calculated from the slope of the plot $\text{Log}_{dc} \sigma$ (S/cm) vs. $1000/T$ (K^{-1}) in the Fig. 7 (c). Shows in the slope value determination plot for the V_2O_5 nanorods prepared at 600°C . The activation energy estimated for PVP surfactants have been listed in the table (2) the increase of PVP from 0.185 eV are present²⁷. The activation energy value (0.27eV) due to the lower ionic size of the V_2O_5 nanorods that could be 0.185 eV the values are in good agreement with the reported values.

5. CONCLUSION

The V_2O_5 nanorods have been successfully prepared by sol-gel techniques. The XRD result revealed that the product is orthorhombic phase in nature. The blue shift observed in the UV-visible spectrum is the typical signature of quantum confinement effect in V_2O_5 nanorods. The PL spectra of V_2O_5 nanorods reveal that the blue-green emission with intensity related to the structural defects. FTIR spectrum conformed that the presence of V_2O_5 functional groups and the formation of V-O bond. HRTEM image reveals clearly the formation of hexagonal nanorods when the V_2O_5 nanorods at 600°C . From AFM analysis, higher surface roughness and RMS value were found out for pure V_2O_5 nanoparticle. The AC conductivity of V_2O_5 samples have been studied in the temperature range 303–393 K and the frequency range from 1 Hz to 5 MHz. The obtained results of AC conductivity were reasonably interpreted in terms of the correlated barrier hopping (CBH) model. The DC electrical conductivity was studied as a function of temperature which indicated the semiconducting nature. Here, on that resistivity decrease and conductivity increase with activation energy studied for the V_2O_5 nanorods.

ACKNOWLEDGEMENTS

Authors wish to express their sincere thanks to the UGC-Rajiv Gandhi National fellowship at New Delhi.

REFERENCE

1. F.J. Morin, Phys. Rev. Lett, 1959; 3: 34-35.
2. H.N. Van, D. Lichtman, J. Vac. Sci. Tech, 1981; 18: 49-53.

3. T. Kudo, Y. Ikeda, T. Watanabe, M. Hibino, M. Miyayama, H. Abe, K. Kajita, *Solid State Ion.*153 (2002)833–841.
4. A. Legrouri, T. Baird, J. R. Fryer, *J.Catal.*1993; 140: 173–183.
5. J. Wu, Y. Zhanq, Y. He, C. Liu, W. Guolt, S. Ruan, *J. Nanosci. Nanotechnol.* 2014;14: 4214–4217.
6. G. T. Kim, J. Muster, V. Krstic, Y. W. Par, S. Roth, M. Burghard, *Appl. Phys. Lett.* 2000; 76:1875–1877.
7. N. Pinna, M. Willinger, K. Weiss, J. Urban, R. Schlogl, *Nano.Lett.*2003; 3: 1131–1134.
8. Z. Wang, J. Chen, X. Hu, *ThinSolidFilms.*2000; 375: 238–241.
9. N. C. S. Vieira, W. Avansi, A. Figueiredo, C. Ribeiro, V. R. Mastelaro, E. Guimaraes, *Nano.Res.Lett.*2012 ; 7: 310-314
10. Yawning, Q. Su, C. H. Chen, M. L. Yu, G. J. Han, G. Q. Wang, K. .Xin, W. Lan, X.Q. Liu, *J. Phys. D: Appl.Phys.*2010; 43: 183001–185402.
11. A. Pan, J. G. Zhang, Z. Nie, G. Cao, B. W. Arey, G. Li, S. Q. Liang, J. Liu, *J. Mater. Chem* 2010 ; 20: 9193-9199.
12. C. Ramana, R. J. Smith, O. M. Hussain, C. M. Julien, *Mater. Sci. Eng. B*2004 ; 11: 218-225.
13. P. Viswanathamurthi, N. Bhattarai, H.Y.Kim,D.R.Lee,*Scr.Mater.*2003; 49:77–581.
14. W. Avansi, C. Ribeiro, E. R. Leite, V. R. Mastelaro, *Crystal Growth and Design* 2009; 9: 3626-3631.
15. J. Muster, G. T. Kim, V. Krstic, J. G. Park, Y. W. Park, S. Roth, M. Burghard. *Advanced Materials* 2000; 12: 420-424.
16. N. Ferrer-Anglada, J. A. Gorri, J. Muster, K. Liu, M. Burghard, S. Roth, *mater scien and engineering: C* 2001; 15: 237-239.
17. M. Zeng, H. Yin, K. Yu, *Chem.Eng.J.*2012 ; 188: 64–70.
18. T.Ivanova,A.Harizanova,T.Koutzatova,B.Vertruyen,*Mater.Lett.*2010 ; 64: 1147–1149.
19. M. H. Mamat, M. Z. Sahdan, Z. Khusaimi, M. Rusop, in *Proceeding so the International Conference on Electronic Devices, Systems and Applications (ICEDSA'10)*,2010; 408–411.
20. A. Talledo, C. G. J. Granq vist, *J.Appl.Phys.*1995 ; 77: 4655–4666.
21. V. Naydenov,L.Tosheva,J.Sterte,*MicroporousMesoporousMater.*2002; 55: 253–263.
22. D. R.W. Briigel, *An introduction to Infrared Spectroscopy*, New York, 1962.
23. N. Nagarani,*J.Photon.Spintron.*2013; 12: 19–21.
24. N. Senthil kumar, M. Sethu raman, J. Chandrasekaran, R. Priya, Murthy Chavali, R. Suresh. *Mater. Scien. in Semi. Processing* 2016; 41: 497-507.
25. K. Funke, *Solid. Stat. Ionics*1997; 94 : 27-33.

26. V. K. Saraswat, K. Singh, N. S. Saxena, V. Kishore, T. P. Sharma, P. K. Saraswat. *Curr. Appl. Phys.* 2006; 6
27. Y. Tominaga, S. Asai, M. Sumita, S. Pamero, B. Scrosati, *J. Power Source* 2005 ; 146: 402-406.